Smart Structures and Systems, *Vol. 27, No. 1 (2021) 123-137*
DOI: https://doi.org/10.12989/sss.2021.27.1.123

Physical test and PFC modelling of rock pillar failure containing two neighboring joints and one hole

V. Sarfarazi*[1], S. Abharian [2a] and A. Ghorbani [2b]

[1] *Department of Mining Engineering, Hamedan University of Technology, Hamedan, Iran*
[2] *Department of Mining and Metallurgical Engineering, Amirkabir University, Tehran, Iran*

(*Received August 6, 2020, Revised September 16, 2020, Accepted September 26, 2020*)

Abstract. Experimental and discrete element methods were used to investigate the effects of both of the non-persistent joints and hole on the failure behaviour of rock pillars under uniaxial compressive test. Concrete samples with dimension of 150 mm × 150 mm × 50 mm were prepared. Within the specimen, two echelon non-persistent notches and one hole were provided. The hole was inserted at the middle of the specimen. two joints were distributed on the three diagonal planes. the angle of diagonal plane related to horizontal axis were 15°, 30° and 45°. The angle of joints related to diagonal plane were 30°, 45°, 60°. Totally, 9 different configuration systems were prepared. In these configurations, the length of joints was taken as 20 mm. diameter of hole was 20 mm. Similar to those for joints configuration systems in the experimental tests, 9 models with different echelon non-persistent joint were prepared in numerical model. The axial load was applied to the model by rate of 0.05 mm/min. the results show that the failure process was mostly governed by both of the non-persistent joint angle and diagonal plane angle. The compressive strengths of the specimens were related to the fracture pattern and failure mechanism of the discontinuities. It was shown that the shear behaviour of discontinuities is related to the number of the induced tensile cracks which are increased by increasing the joint angle. The strength of samples increases by increasing both of the joint angle and diagonal plane angle. The failure pattern and failure strength are similar in both methods i.e., the experimental testing and the numerical simulation methods.

Keywords: PFC2D; physical test; echelon non-persistent joint; joint angle; hole

1. Introduction

Pillars are used in a mine to support the weight of overburden material between adjacent underground openings. As mine depths increase, pillar failure becomes more frequent and critical due to the progressive increase in ambient stresses (Cook 1976). This failure process is a progressive one due to the initiation and propagation of cracks, disturbance of local stress fields, development of local failures and the formation of fracture planes. These micro processes lead to macroscopic pillar failure and the associated loss of load-carrying capability (Fang and Harrison 2002). The feature of pillars in fractured rock mass is their complex mechanical behavior due to the fact that the rock mass is a geological formation that is represented by a set of blocks of one or more types of rock mass separated by cracks of various nature (Protosenya and Verbilo 2016). Thus, the strength and deformation properties of a pillar are determined by the presence of defects and disruptions in it, and their characteristics (Ranjith *et al*. 2004). Methods of calculating mechanical characteristics of the fractured rock mass may be divided into direct and indirect (Khani 2013). Direct methods include experiments in the laboratory and in the field (Kulatilake and Stephansson 1994). The test results obtained in the laboratory conditions for limited dimensions of samples do not reflect the real properties of the rock mass, the dimensions of which greatly exceed those of laboratory samples. On the other hand, samples of larger dimensions may be tested. It is worth noting that this process requires more labor, higher costs and is technically difficult to implement (Coli *et al*. 2011) since the possibilities of choosing dimensions of the rock mass for testing are limited. Another important disadvantage of this approach is the invisibility of the initial cracks and uncertainty of the boundary conditions, which eliminates the possibility of determining the required dependencies. Indirect methods are divided into analytical (Halakatevakis and Sofianos 2010), empirical (Hoek and Brown 1997, Özkan *et al*. 2015, Palmstrom and Singh 2001), experimental (Sarfarazi *et al*. 2014, 2016, 2017, Sarfarazi and Haeri 2016, Haeri and Sarfarazi 2016a-c, Haeri *et al*. 2016, Lin *et al*. 2020), and numerical (Yang *et al*. 2015, Min and Jing 2003, Yaylaci and Avcar 2020), with each having its advantages and disadvantages. The empirical approach allows only limited conservative estimation based on previous construction experience, moreover, it has no mathematical basis, but today it is widely used, as allows to obtain quantitative indicators of the strength and deformation properties of rock mass based on qualitative characteristics. Although this method is used in the world

*Corresponding author, Associate Professor,
E-mail: vahab.sarfarazi@gmail.com
[a] Research Scholar
[b] Research Scholar

ISSN: 1738-1584 (Print), 1738-1991 (Online)

practice, its use makes it impossible to present the anisotropy of properties in the tensor form (Gerrard 1982, Amadei 1988). Analytical methods of analysis reduce uncertainty in assessing the properties of the fractured rock mass, and allow displaying anisotropy of properties, compared to the empirical methods. However, the main disadvantage of the analytical methods is the impossibility of accounting for geometrically complex fracture systems, which are typical for real fractured rock mass. In recent decades, the focus of researchers' attention has been gradually shifting to the numerical methods of determining mechanical parameters of the fractured mass, due to the active development of computer technologies and increasing their computing abilities (Yang *et al*. 2015, Min and Jing 2003, Esmaieli *et al*. 2010, Ivars *et al*. 2011, Martina and Maybee 2000, Yaylaci 2016, Yaylaci and Birinci 2013, 2015, Yaylaci *et al*. 2019, Yaylaci *et al*. 2020). In this study, uniaxial tests for rock masses containing one hole and two joints are carried out using experimental test and numerical simulations. Two parameters were changed i.e., Joint angle and diagonal plane angle. The evolutions of the failure pattern and uniaxial compressive stresses with different joint dip angles and diagonal plane angles have been estimated.

2. Uniaxial compression test for rock-like specimens with echelon joint

Rock-like materials were used for simulating fractured rock masses in these tests. The materials were mixed according to a mass ratio of 2:1 of anchor cement: water. The sample size (length × width × height) was 15 cm × 10 cm × 5 cm. open cracks was made by pre-inserting a thin metal sheet and pulling the sheet outward after the initial solidification of the specimen. To eliminate accidental error and enhance the scientific experiment, three identical prefabricated crack test blocks were prepared for each group. Echelon non-persistent cracks were formed in the model. The prefabricated crack in this experiment was 1 mm wide and 20 mm long. The specimens were placed in a cool and ventilated location for 28 days (Fig. 1).

The dip angle of the diagonal plane, which is an angle between the axis of the diagonal plane and the horizontal direction, is indicated in Fig. 2. Diagonal plan angles were 30°, 45° and 60°. The angle of three joints related to diagonal plane were 15°, 30° and 45°. 9 types of echelon joints configuration were used in this experiment. The crack arrangement and specimen number of each specimen were depicted in Fig. 3. The uniaxial compression test for the non-persistent joints was performed using the electrohydraulic universal testing machine. The experimental system consists of test bed, loading control system and data acquisition system. The specimen was placed in the center of the base and kept horizontal contact with the base. During the experiment, the displacement loading rate was controlled to 0.05 mm/min (Fig. 4).

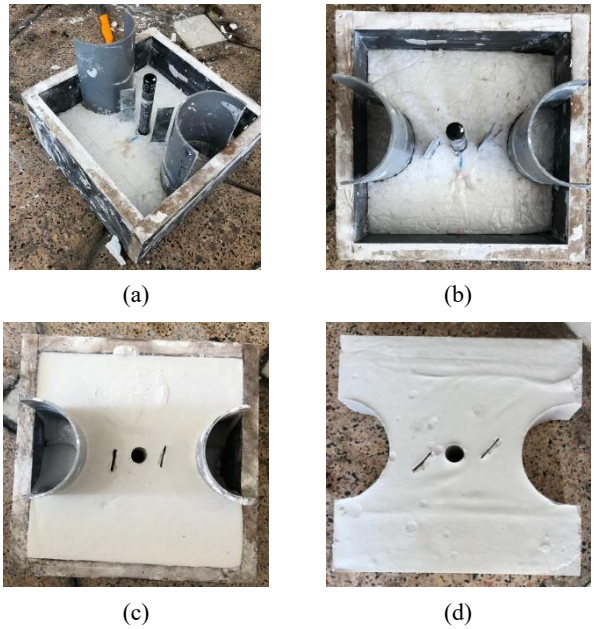

(a) (b) (c) (d)

Fig. 1 (a) The frame with dimension of 150 mm × 100 mm × 50 mm, a special plastic fiber with dimension of 150 mm × 100 mm × 50 mm was put into the frame, the shim inside the plastic fiber; (b) adjustment the shim inside the frame; (c) adjustment the shim inside the frame; (d) the aluminum sheet is removed from the mold

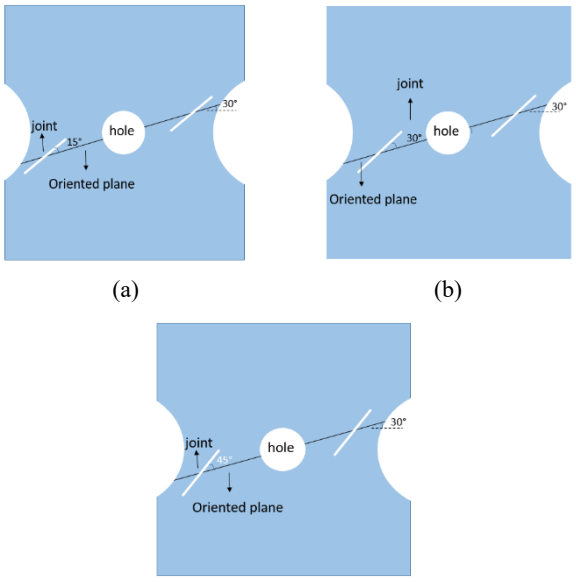

(a) (b) (c)

Fig. 2 (a) Oriented plane angle was equal to 30° and joint angle was 15°, (b) oriented plane angle was equal to 30° and joint angle was 30°, (c) oriented plane angle was equal to 30° and joint angle was 45°. (d) oriented plane angle was equal to 45° and joint angle was 15°, (b) oriented plane angle was equal to 45° and joint angle was 30°, (c) oriented plane angle was equal to 45° and joint angle was 45°; oriented plane angle was equal to 45. (a) oriented plane angle was equal to 60° and joint angle was 15°, (b) oriented plane angle was equal to 60° and joint angle was 30°, (c) oriented plane angle was equal to 60° and joint angle was 45°

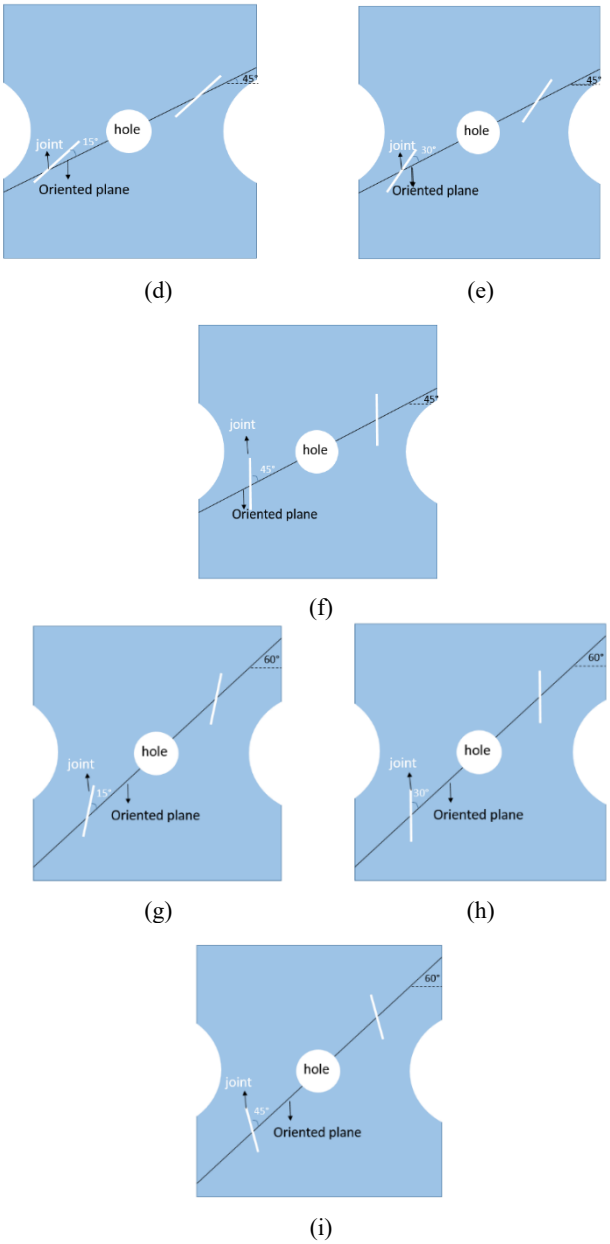

Fig. 2 Continued

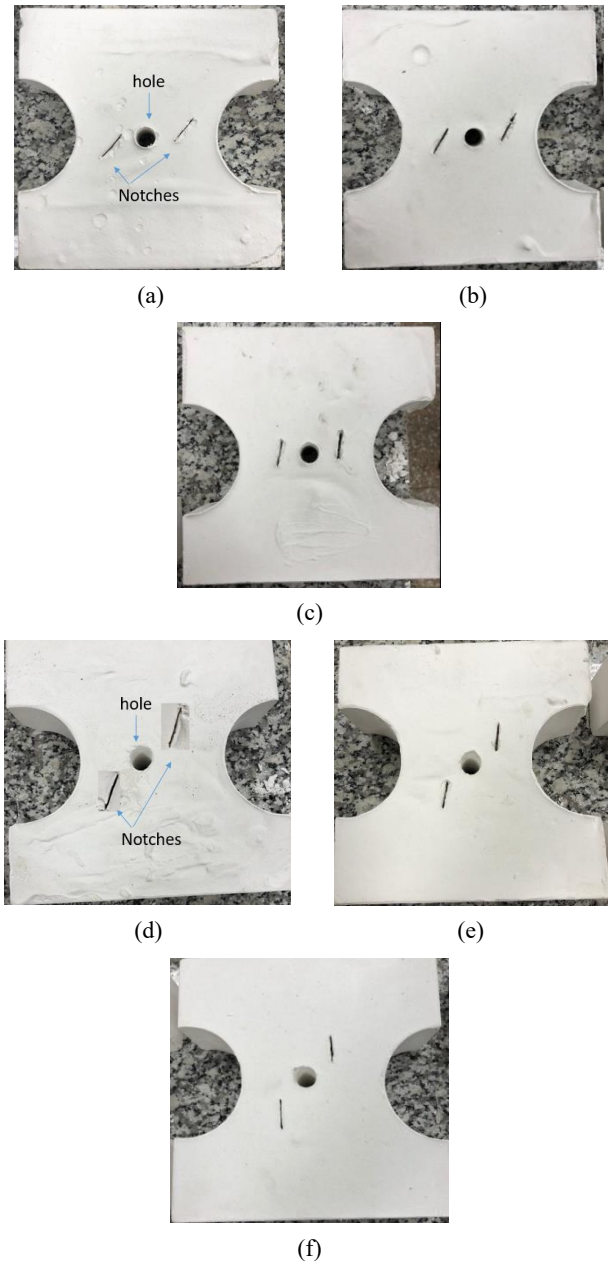

Fig. 3 (a) Oriented plane angle was equal to 30° and joint angle was 15°, (b) oriented plane angle was equal to 30° and joint angle was 30°, (c) oriented plane angle was equal to 30° and joint angle was 45°. (d) oriented plane angle was equal to 45° and joint angle was 15°, (b) oriented plane angle was equal to 45° and joint angle was 30°, (c) oriented plane angle was equal to 45° and joint angle was 45°; oriented plane angle was equal to 45°. (a) oriented plane angle was equal to 60° and joint angle was 15°, (b) oriented plane angle was equal to 60° and joint angle was 30, (c) oriented plane angle was equal to 60° and joint angle was 45°

3. Experimentally observed failure patterns

In this study, some experimental work was carried out to observe the failure pattern of the specimens containing non-persistence joints with different joint angle.

3.1 Failure pattern of experimental specimens

a) Oriented plane angle was 30

Fig. 5 shows the failure pattern of specimens with oriented plane angle of 30°. When joint angle was 15° (Fig. 5(a)), two tensile wing cracks initiated from outer joint tips and propagated diagonally related to loading axis till coalescence with boundaries of sample. Also, two wing crack initiate from inner joint tips and propagates diagonally till coalescence with the hole wall. Two vertical tensile cracks initiate from the joint walls and propagate parallel to loading axis till coalescence with sample boundary. When joint angle was 30° (Fig. 5(b)), one tensile wing cracks initiated from outer tip of left joint and propagated diagonally related to loading axis till coalescence with boundaries of sample. Also, two vertical

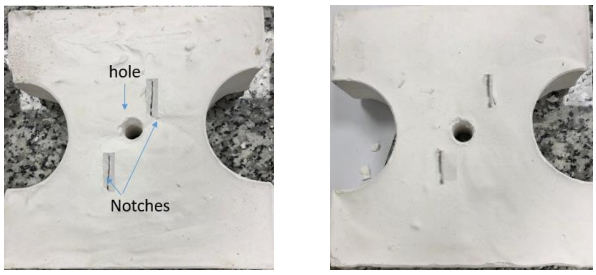

(g) (h)

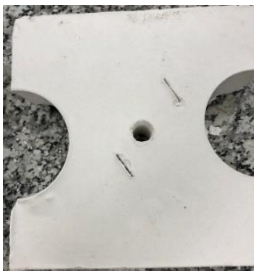

(i)

Fig. 3 Continued

Fig. 4 Specimen are placed between the plates of the loading machine

tensile cracks initiate from the joint walls and propagate parallel to loading axis till coalescence with sample boundary. When joint angle was 45° (Fig. 5(c)), one tensile wing cracks initiated from outer tip of right joint and propagated diagonally related to loading axis till coalescence with boundaries of sample. Also, two vertical tensile cracks initiate from the joint walls and propagate parallel to loading axis till coalescence with sample boundary. In these conditions, the rock bridges were broken during the test. Failure surface was smooth without pulverized material. This is representative of tensile crack.

b) Oriented plane angle was 45

Fig. 6 shows the failure pattern of specimens with oriented plane angle of 30°. When joint angle was 15° (Fig. 6(a)), two tensile wing cracks initiated from inner joint tips and propagated diagonally related to loading axis till coalescence with boundaries of hole. Two vertical tensile cracks initiate from the joint walls and propagate parallel to loading axis till coalescence with sample boundary. When

(a) (b)

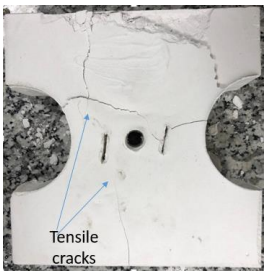

(c)

Fig. 5 Failure pattern in specimens containing three echelon joint with angle of; (a) 15°; (b) 30°; (c) 45°; oriented plane angle was equal to 30

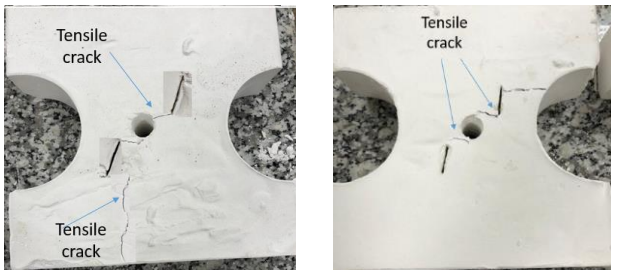

(a) (b)

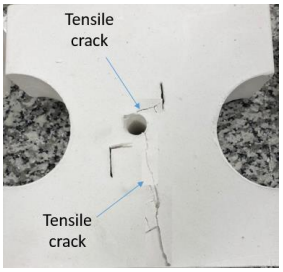

(c)

Fig. 6 Failure pattern in specimens containing three echelon joint with angle of; (a) 15°; (b) 30°; (c) 45°; oriented plane angle was equal to 45

large joint angle was 30° (Fig. 6(b)), two tensile wing cracks initiated from outer joint tips and propagated diagonally related to loading axis till coalescence with boundaries of sample. Also, two wing crack initiate from inner joint tips and propagates diagonally till coalescence with the hole wall. When large joint angle was 45° (Fig. 6(c)), two tensile wing cracks initiated from inner joint tips and propagated diagonally related to loading axis till coalescence with boundaries of hole. Two vertical tensile cracks initiate from the joint walls and propagate parallel to

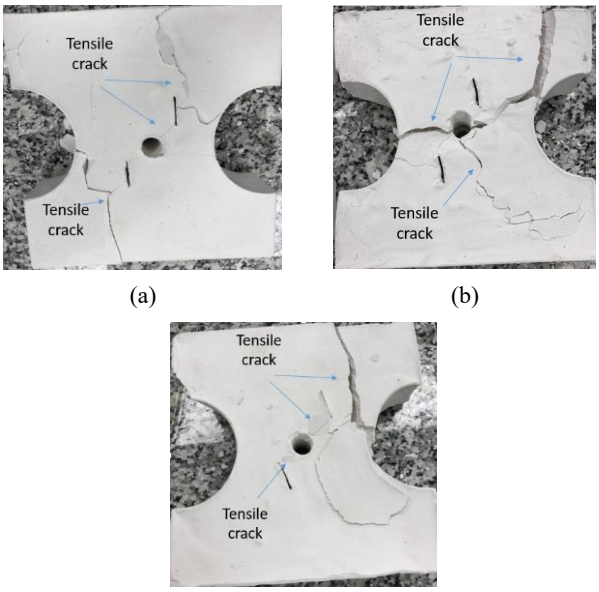

Fig. 7 Failure pattern in specimens containing three echelon joint with angle of; (a) 15°; (b) 30°; (c) 45°; oriented plane angle was equal to 60

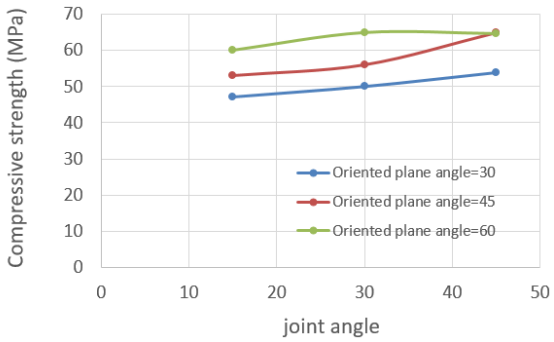

Fig. 8 The effect of joint angle on the strength of models

loading axis till coalescence with sample boundary. In these conditions, the rock bridges were broken during the test. Failure surface was smooth without pulverized material. This is representative of tensile crack.

c) Oriented plane angle was 60

Fig. 7 shows the failure pattern of specimens with oriented plane angle of 60°. When joint angle was 15° (Fig. 7(a)), two tensile wing cracks initiated from outer joint tips and propagated diagonally related to loading axis till coalescence with boundaries of sample. Also, two wing crack initiate from inner joint tips and propagates diagonally till coalescence with the hole wall. Two vertical tensile cracks initiate from the joint walls and propagate parallel to loading axis till coalescence with sample boundary. When joint angle was 30° (Fig. 7(b)), one tensile wing cracks initiated from outer tip of left joint and propagated diagonally related to loading axis till coalescence with boundaries of sample. Also, two vertical tensile cracks initiate from the joint walls and propagate parallel to loading axis till coalescence with sample boundary. When joint angle was 45° (Fig. 7(c)), one tensile wing cracks initiated from outer tip of right joint and propagated diagonally related to loading axis till coalescence with boundaries of sample. Also, two vertical tensile cracks initiate from the joint walls and propagate parallel to loading axis till coalescence with sample boundary. In these conditions, the rock bridges were broken during the test. Failure surface was smooth without pulverized material. This is representative of tensile crack.

3.2 The effect of oriented plane angle and joint angle on the strength of samples

Fig. 8 shows the effect of oriented plane angle and joint angle on the strength of models. This figure was presented for three oriented plane angle. The strength of samples was increased by increasing the joint angle. Also, the strength of sample was increased by increasing the oriented plane angle.

4. Numerical model

4.1 Particle flow code

The PFC2D model is a collection of discrete circular particles and uses the explicit time-step circulation rule to calculate the model particles cyclically (Cundall and Strack 1979). The contact force between particles obeys the law of force–displacement, particles motion is based on the Newton's second law. As a discrete element model (DEM), the bond particle model contains two main types of models namely "contact bond model" and "parallel bond model". In the contact bond model, particles are joined by a point of glue and contacts cannot transfer moment. While in the parallel bond model particles are joined by an area of glue and contacts can resist moment induced by particle rotation. Thus the parallel bond model can represent a cement-like substance (Fig. 9), such as rock (Potyondy and Cundall 2004). The force between particles is reflected through the contact force chain and a bond breakage will occur and forms micro cracks when the local stresses exceed the parallel bond strength.

4.2 Preparation and calibration of the PFC2D model for rock-like material

The standard process of generating a PFC2D assembly to represent a test model, used in this article, is described in

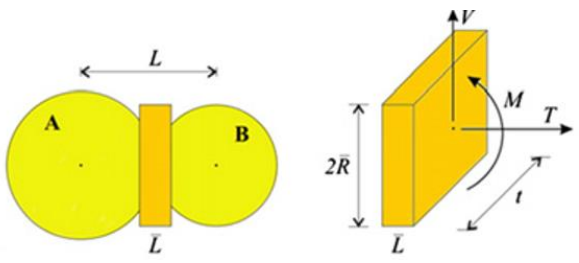

Fig. 9 Force–displacement behavior of the grain-bonding system after, Potyondy and Cundall 2004

Table 1 Micro properties used to represent the intact rock

Parameter	Value	Parameter	Value
Type of particle	Disc	Parallel-bond radius multiplier	1
Density (kg/m^3)	3000	Young's modulus of parallel bond (GPa)	33
Minimum radius (mm)	0.27	Parallel bond stiffness ratio	1.7
Size ratio	1.56	Particle friction coefficient	0.4
Porosity ratio	0.08	Parallel bond normal strength, mean (MPa)	75
Damping coefficient	0.7	Parallel bond normal strength, SD (MPa)	10
Contact Young's modulus (GPa)	33	Parallel bond shear strength, mean (MPa)	75
Stiffness ratio	1.7	Parallel bond shear strength, SD (MPa)	10

detail by Potyondy and Cundall (2004). The process involves: particle generation, packing the particles, isotropic stress installation (stress initialization), floating particle (floater) elimination and bond installation. A gravity effect did not need to be considered as the specimens were small, and the gravity-induced stress gradient had a negligible effect on the macroscopic behavior. Uniaxial compressive strength and Brazilian test were carried out to calibrate the properties of particles and parallel bonds in bonded particle model (Ghazvinian *et al*. 2012). Adopting the micro-properties listed in Table 1 and the standard calibration procedures (Potyondy and Cundall 2004), a calibrated PFC particle assembly was created. Figs. 14(a) and (b) shows the experimental uniaxial compression test and numerical simulation, respectively. Figs. 14(c) and (d) shows experimental Brazilian test and numerical simulation, respectively. The results show well matching between experimental test and numerical simulation. Also, the obtained specimen properties from the numerical models such as elastic modulus, Poisson's ratio, UCS values agree well with the experimental values, as indicated in Table 2.

4.3 Numerical compressive tests on the non-persistent open joint

After calibration of PFC2D, uniaxial tests for jointed rock were numerically simulated by creating a box model in the PFC2D (by using the calibrated micro-parameters) (Fig. 11). The PFC specimen had the dimensions of 100 mm × 100 mm. A total of 13438 disks with a minimum radius of 0.27 mm were used to make the box specimen. Two walls exist at the upper and lower of the model. The non-persistent joints were formed by deletion of bands of particles from the model (Fig. 11). The dip angle of the diagonal plane, which is an angle between the axis of the diagonal plane and the horizontal direction, is indicated in Fig. 2. Diagonal plan angles were 30°, 45° and 60°. The

Table 2 Comparison of macro-mechanical properties between experiments and model

Mechanical properties	Experimental results	PFC2D Model results
Elastic modulus, (GPa)	30	32
Poisson's ratio	0.18	0.19
UCS, (MPa)	74	74.4
Brazilian tensile strength (MPa)	5	5.2

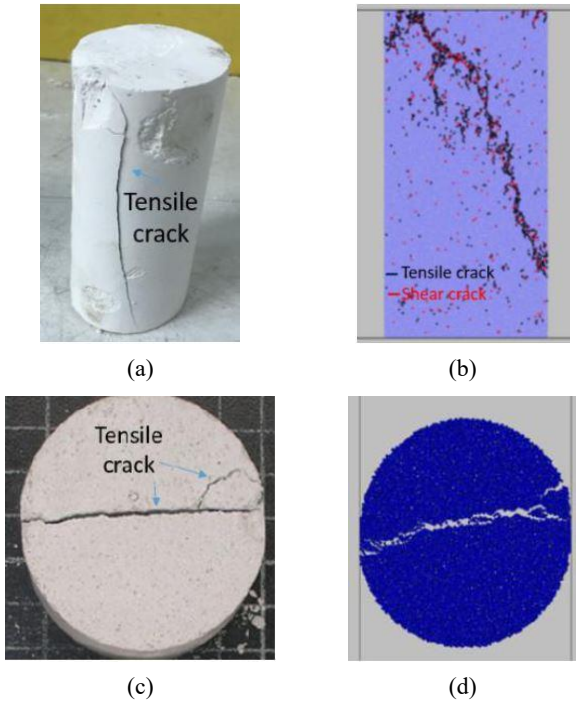

Fig. 10 (a) Experimental compression test; (b) numerical compression test; (c) experimental Brazilian test; and (d) numerical Brazilian test.

angle of three joints related to diagonal plane were 15°, 30° and 45°. 9 types of Y shape non-persistent joints were used in this numerical simulation. The crack arrangement and specimen number of each specimen were depicted in Fig. 11. It should be noticed that this joint configuration is similar to experimental one. Upper and lower walls applied uniaxial force on the model. The compression force was registered by taking the reaction forces on the upper wall.

4.4 The modelled parallel bond forces before the crack initiation process

The parallel bond force distribution (as shown in Figs. 12-14) illustrates the state of force vectors within the modelled samples before the crack initiation process. The red and dark lines shown in Figs. 12-14 represent the tensile and compression force vectors in the model, respectively. The coarse lines and their accumulation show the areas where larger forces are induced within the model.

It can be easily seen that the tensile forces of the bonded particles at the tip of the crack are more than their shear

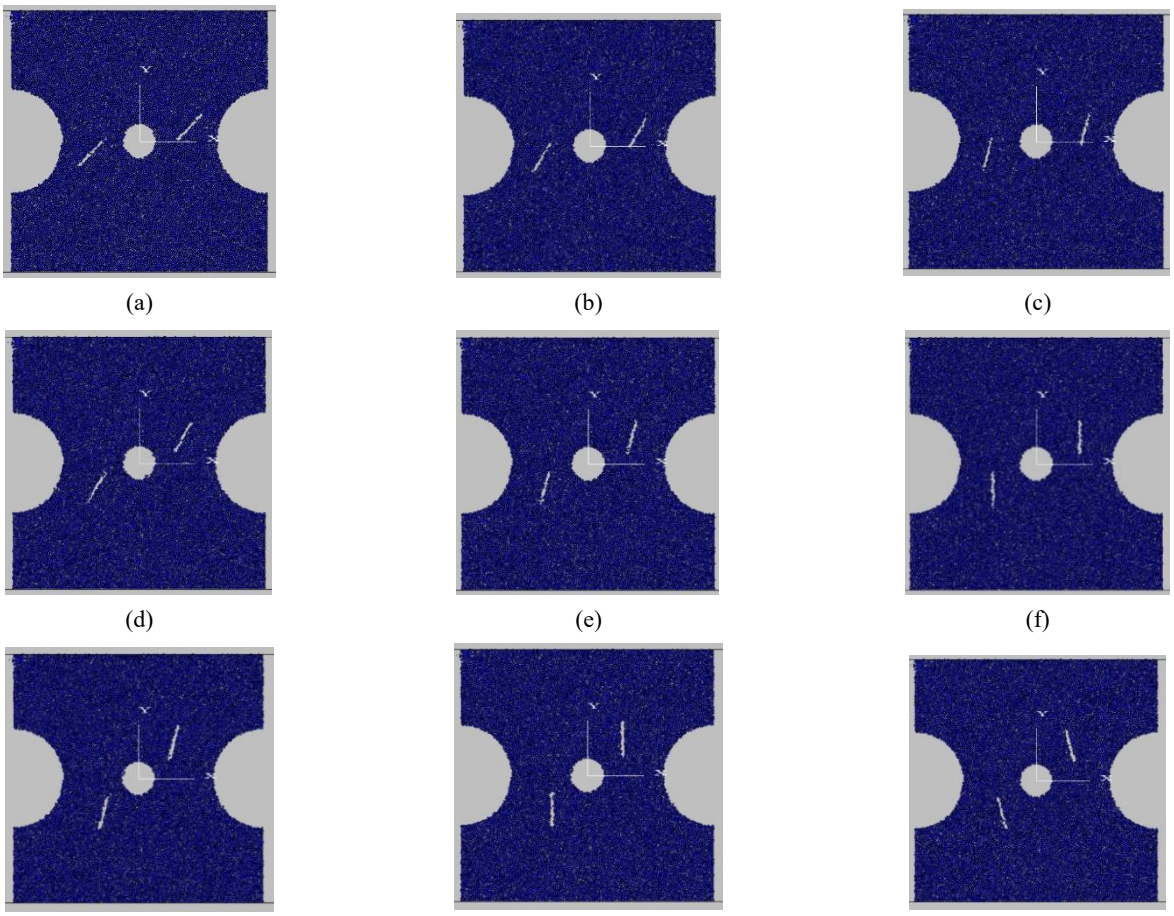

(a) (b) (c)

(d) (e) (f)

(g) (h) (i)

Fig. 11 (a) oriented plane angle was equal to 30° and joint angle was 15°, (b) oriented plane angle was equal to 30° and joint angle was 30°, (c) oriented plane angle was equal to 30° and joint angle was 45°. (d) oriented plane angle was equal to 45° and joint angle was 15°, (e) oriented plane angle was equal to 45° and joint angle was 30°, (f) oriented plane angle was equal to 45° and joint angle was 45°; oriented plane angle was equal to 45°. (g) oriented plane angle was equal to 60° and joint angle was 15°, (h) oriented plane angle was equal to 60° and joint angle was 30, (i) oriented plane angle was equal to 60° and joint angle was 45

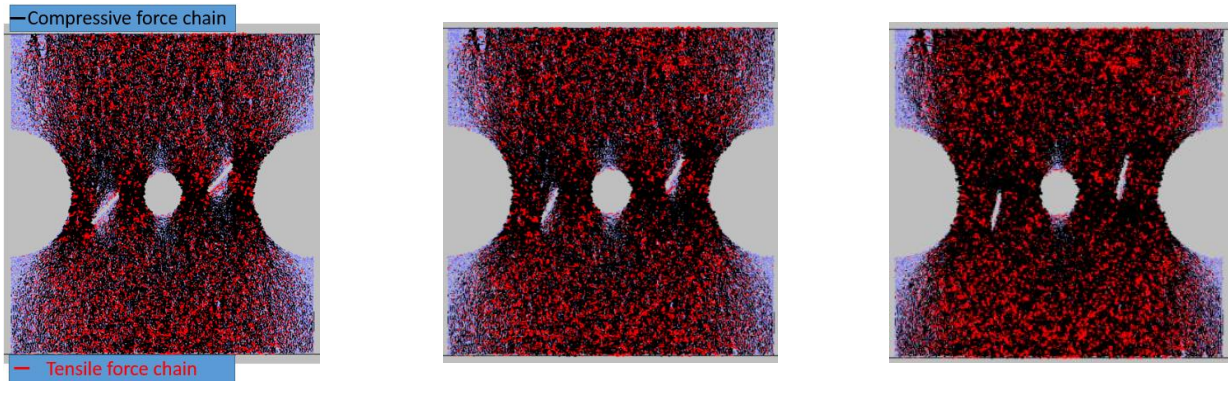

(a) (b) (c)

Fig. 12 Parallel bond force distribution in the model with in specimens two echelon joint with angle of; (a) 15°; (b) 30°; (c) 45°; oriented plane angle was equal to 30°

strength, therefore, the tensile crack initiation is a dominant mode of fracturing that initiates at the tip of the crack within the modelled samples. It's to be noticed that when the joint angle was 30, maximum tensile force at tip of the joints is more than another configuration. Fig. 15 shows the variation of value of maximum tensile force at the joint tip based on joint angle for time step of 400 cycle. The trends have been shown for three oriented plane angles. The value

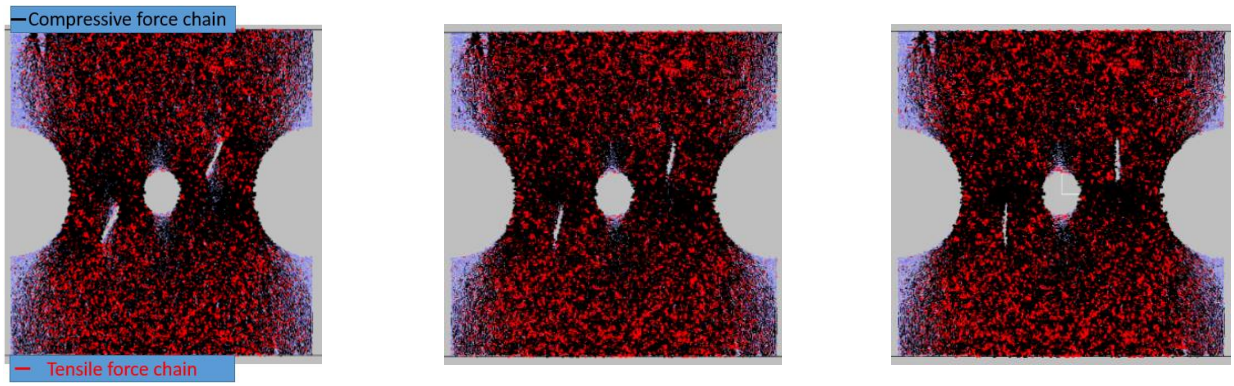

(a) (b) (c)

Fig. 13 Parallel bond force distribution in the model with in specimens two echelon joint with angle of; (a) 15°; (b) 30°; (c) 45°; oriented plane angle was equal to 45°

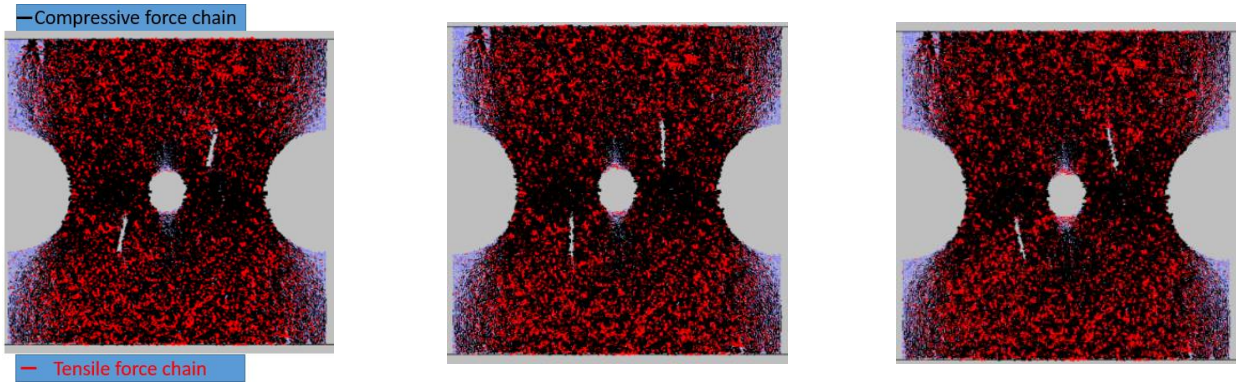

(a) (b) (c)

Fig. 14 Parallel bond force distribution in the model with in specimens two echelon joint with angle of; (a) 15°; (b) 30°; (c) 45°; oriented plane angle was equal to 45°

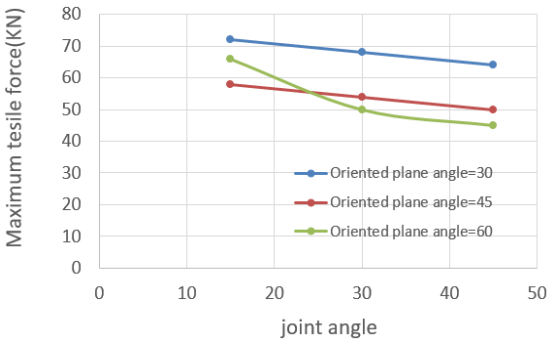

Fig. 15 The variation of value of maximum tensile force at the joint tip based on joint angle for time step of 400 cycle

of maximum tensile force is decreased by increasing the joint angle. Also, the value of maximum tensile force is decreased by increasing the oriented plane angle. It means that when joint angle has low value, the maximum tensile force concentration at the joint tip is too high and crack initiate at low far field compressive force. Also, when oriented plane angle has low value, the maximum tensile force concentration at the joint tip is too high and crack initiate at low far field compressive force.

4.5 Failure mechanism of numerical model

a) Oriented plane angle was 30°

a-1) joint angle was 15°

Figs. 16(a)-(c) shows the failure mechanism of specimens with oriented plane angle of 30° and joint angle of 15° in three stages of loading i.e., crack initiation stress stage, final stress stage and post peak stress stage. Red line and black line were representative of shear crack and tensile crack, respectively. Fig. 16(d) shows the variation of compressive stress versus the cycle. Three loading stages were highlighted in this figure. In crack initiation stage (Fig. 16(a)), two tensile wing crack initiate from outer tips of joints and propagate diagonally till coalescence with model boundary. In this stage oscillation start in the stress curve ("a" in Fig. 16(d)). In peck stress stage (Figs. 16(b) and (d)), two tensile wing crack initiate from inner tips of joints and propagate diagonally till coalescence with hole boundary. In final stage (Figs. 16(c) and (d)), two tensile wing cracks initiate preexisting joints and propagate parallel to loading axis till coalescence with model boundary.

a-2) joint angle was 30°

Figs. 17(a)-(c) shows the failure mechanism of specimens with oriented plane angle of 30° and joint angle

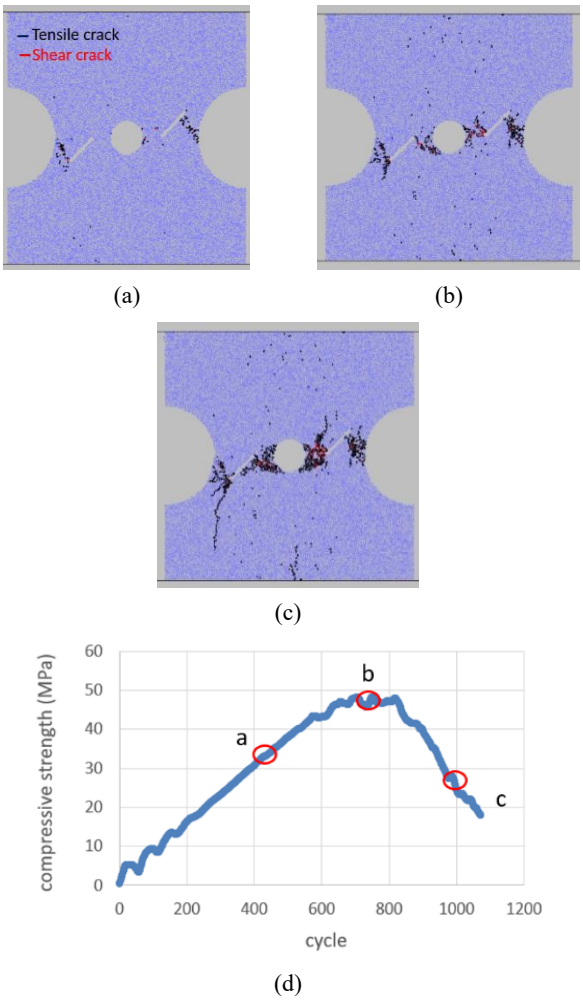

Fig. 16 Crack evolution in specimen containing two echelon joint with angle of 15° during the three stages of the loading; (a) crack initiation stress, (b) peak stress, (c) post peak; oriented plane angle was equal to 30°. (d) Variation of compressive strength versus the cycle

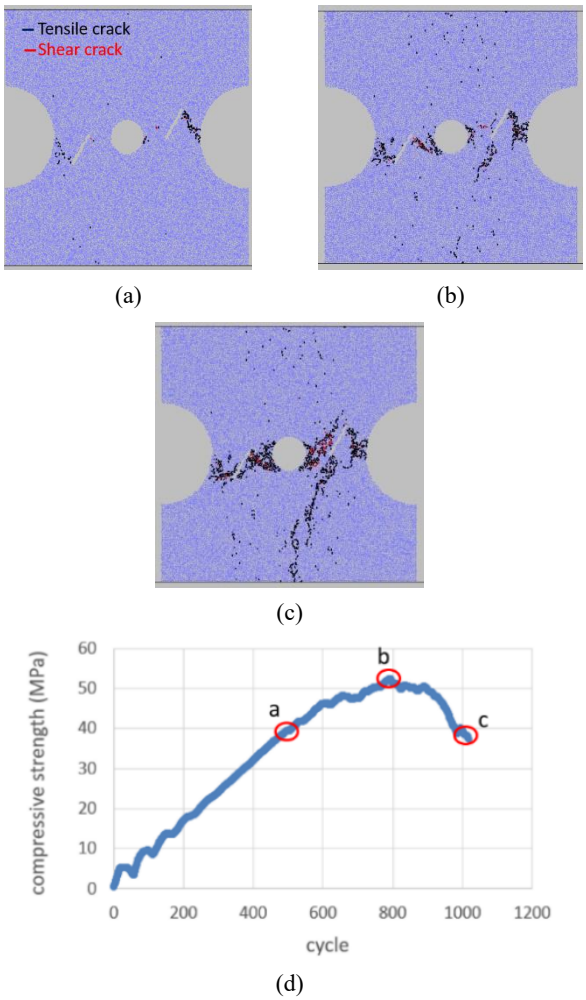

Fig. 17 Crack evolution in specimen containing two echelon joint with angle of 30° during the three stages of the test; (a) crack initiation stress, (b) peak stress, (c) post peak; oriented plane angle was equal to 30°. (d) Variation of compressive strength versus the cycle

of 30° in three stages of loading i.e., crack initiation stress stage, final stress stage and post peak stress stage. Red line and black line were representative of shear crack and tensile crack, respectively. Fig. 17(d) shows the variation compressive stress versus the cycle. Three loading stages were highlighted in this figure.

In crack initiation stage (Fig. 17(a)), two tensile wing cracks initiate from outer tips of joints and propagate diagonally till coalescence with model boundary. In this stage oscillation start in the stress curve ("a" in Fig. 17(d)). In peck stress stage (Figs. 17(b) and (d)), two tensile wing crack initiate from inner tips of joints and propagate diagonally till coalescence with hole boundary. In final stage (Figs. 17(c) and (d)), one tensile wing cracks initiate preexisting joints and propagate parallel to loading axis till coalescence with model boundary.

a-3) joint angle was 45°

Figs. 18(a)-(c) shows the failure mechanism of specimens with oriented plane angle of 30° and joint angle of 45° in three stages of loading i.e., crack initiation stress stage, final stress stage and post peak stress stage. Red line and black line were representative of shear crack and tensile crack, respectively. Fig. 18(d) shows the variation compressive stress versus the cycle. Three loading stages were highlighted in this figure.

In crack initiation stage (Fig. 18(a)), two tensile wing crack initiate from outer tips of joints and propagate diagonally till coalescence with model boundary. In this stage oscillation start in the stress curve ("a" in Fig. 18(d)). In peck stress stage (Figs. 18(b) and (d)), two tensile wing crack initiate from inner tips of joints and propagate diagonally till coalescence with hole boundary. In final stage (Figs. 18(c) and (d)), two tensile wing cracks initiate preexisting joints and propagate parallel to loading axis till coalescence with model boundary.

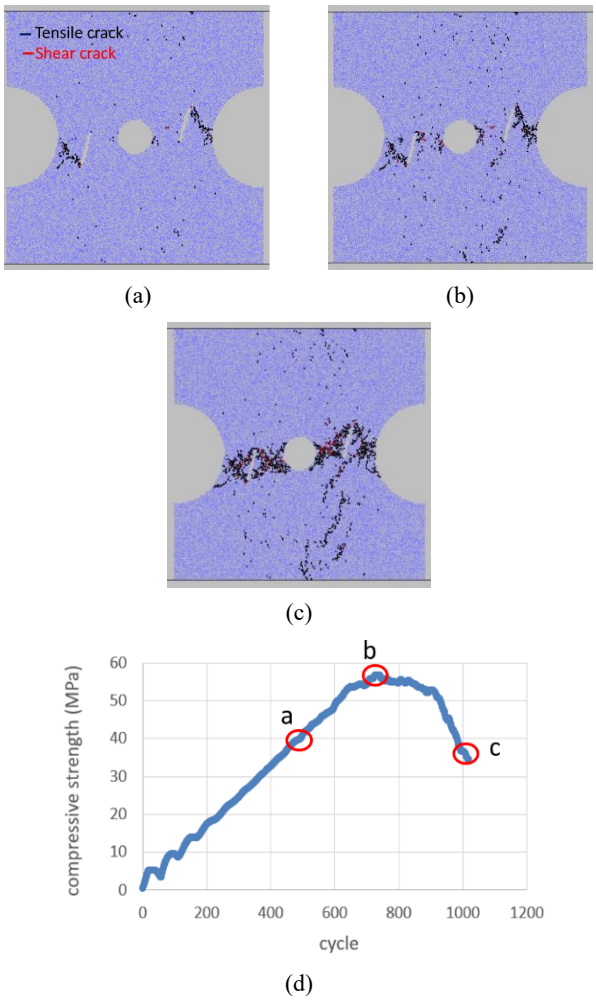

Fig. 18 Crack evolution in specimen containing two echelon joint with angle of 45° during the three stages of the test;(a) crack initiation stress, (b) peak stress, (c) post peak; oriented plane angle was equal to 30°. (d) Variation of compressive strength versus the cycle

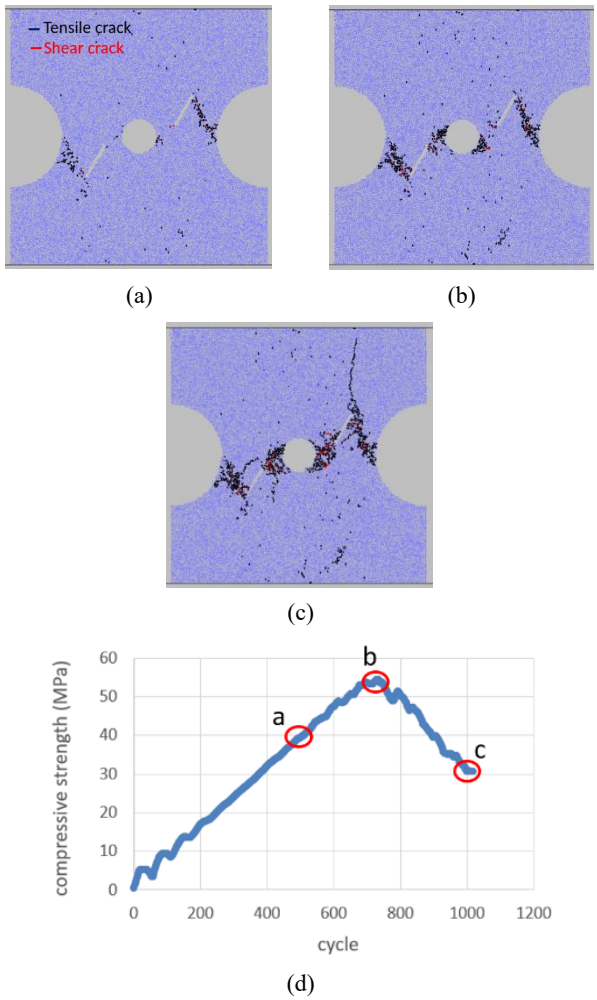

Fig. 19 Crack evolution in specimen containing two echelon joint with angle of 15° during the three stages of the test; (a) crack initiation stress, (b) peak stress, (c) post peak; oriented plane angle was equal to 45°. (d) Variation of compressive strength versus the cycle

b) Oriented plane angle was 45°

b-1) joint angle was 15°

Figs. 19(a)-(c) shows the failure mechanism of specimens with oriented plane angle of 45° and joint angle of 15° in three stages of loading i.e., crack initiation stress stage, final stress stage and post peak stress stage. Red line and black line were representative of shear crack and tensile crack, respectively. Fig. 19(d) shows the variation compressive stress versus the cycle. Three loading stages were highlighted in this figure.

In crack initiation stage (Fig. 19(a)), two tensile wing crack initiate from outer tips of joints and propagate diagonally till coalescence with model boundary. In this stage oscillation start in the stress curve ("a" in Fig. 19(d)). In peck stress stage (Figs. 19(b) and (d)), two tensile wing crack initiate from inner tips of joints and propagate diagonally till coalescence with hole boundary. In final stage (Figs. 19(c) and (d)), two tensile wing cracks initiate preexisting joints and propagate parallel to loading axis till coalescence with model boundary.

b-2) joint angle was 30°

Figs. 20(a)-(c) shows the failure mechanism of specimens with oriented plane angle of 45° and joint angle of 30°in three stages of loading i.e., crack initiation stress stage, final stress stage and post peak stress stage. Red line and black line were representative of shear crack and tensile crack, respectively. Fig. 20(d) shows the variation compressive stress versus the cycle. Three loading stages were highlighted in this figure.

In crack initiation stage (Fig. 20(a)), two tensile wing crack initiate from outer tips of joints and propagate diagonally till coalescence with model boundary. In this stage oscillation start in the stress curve ("a" in Fig. 31(a)). In peck stress stage (Figs. 20(b) and (d)), two tensile wing crack initiate from inner tips of joints and propagate diagonally till coalescence with hole boundary. In final stage (Figs. 20(c) and (d)), two tensile wing cracks initiate preexisting joints and propagate parallel to loading axis till coalescence with model boundary.

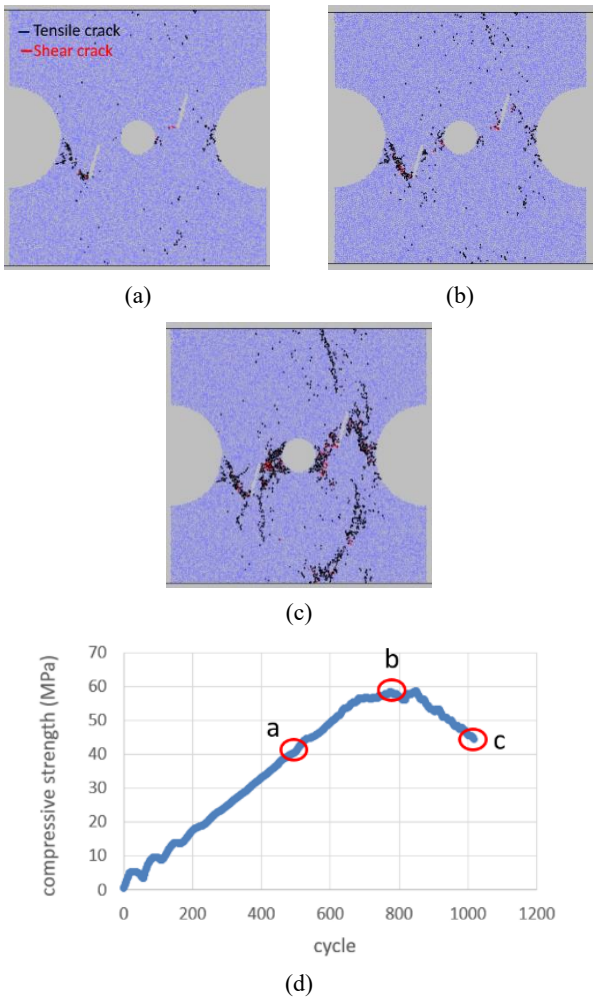

Fig. 20 Crack evolution in specimen containing two echelon joint with angle of 30° during the three stages of the test; (a) crack initiation stress, (b) peak stress, (c) post peak; oriented plane angle was equal to 45°. (d) Variation of compressive strength versus the cycle

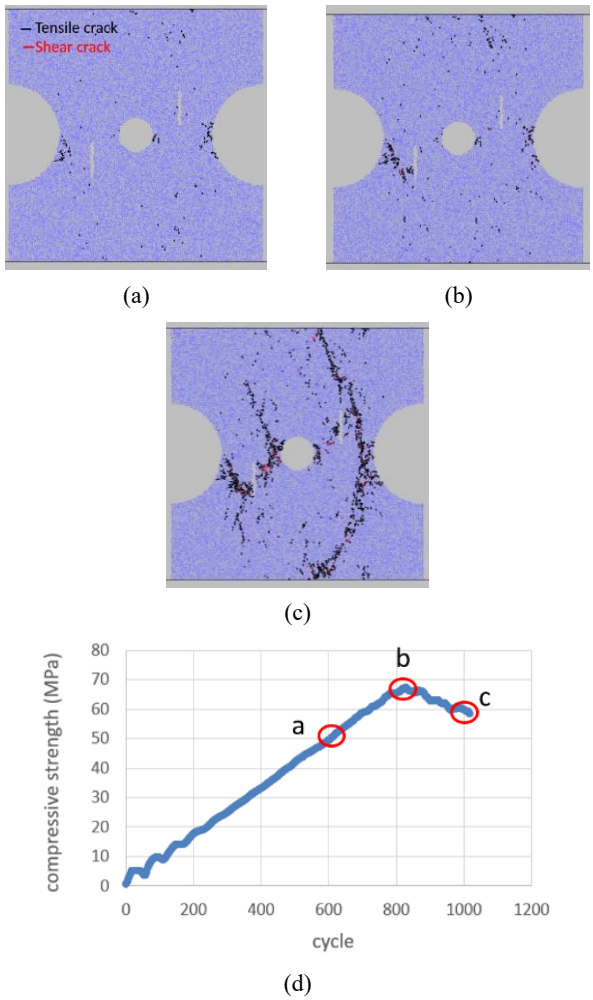

Fig. 21 Crack evolution in specimen containing two echelon joint with angle of 45° during the three stages of the test; (a) crack initiation stress, (b) peak stress, (c) post peak; oriented plane angle was equal to 45°. (d) Variation of compressive strength versus the cycle

b-3) joint angle was 45°

Figs. 21(a)-(c) shows the failure mechanism of specimens with oriented plane angle of 30° and joint angle of 45° in three stages of loading i.e., crack initiation stress stage, final stress stage and post peak stress stage. Red line and black line were representative of shear crack and tensile crack, respectively. Fig. 21(d) shows the variation compressive stress versus the cycle. Three loading stages were highlighted in this figure.

In crack initiation stage (Fig. 21(a)), two tensile wing crack initiate from outer tips of joints and propagate diagonally till coalescence with model boundary. In this stage oscillation start in the stress curve ("a" in Fig. 21(d)). In peck stress stage (Figs. 21(b) and (d)), two tensile wing crack initiate from inner tips of joints and propagate diagonally till coalescence with hole boundary. In final stage (Figs. 21(c) and (d)), two tensile wing cracks initiate preexisting joints and propagate parallel to loading axis till coalescence with model boundary.

c) Oriented plane angle was 60°

c-1) joint angle was 15°

Figs. 22(a)-(c) shows the failure mechanism of specimens with oriented plane angle of 60° and joint angle of 15° in three stages of loading i.e., crack initiation stress stage, final stress stage and post peak stress stage. Red line and black line was representative of shear crack and tensile crack, respectively. Fig. 22(d) shows the variation compressive stress versus the cycle. Three loading stages were highlighted in this figure. In crack initiation stage (Fig. 22(a)), two tensile wing crack initiate from hole walls and propagate diagonally inside the model. In this stage oscillation start in the stress curve ("a" in Fig. 22(d)). In peck stress stage (Figs. 22(b) and (d)), two tensile wing crack initiate from outer tips of joints and propagate diagonally till coalescence with model boundary. Also, two tensile wing crack initiate from inner tips of joints and propagate diagonally till coalescence with hole boundary. In final stage (Figs. 22(c) and (d)), two tensile wing cracks initiate preexisting joints and propagate parallel to loading axis till coalescence with model boundary.

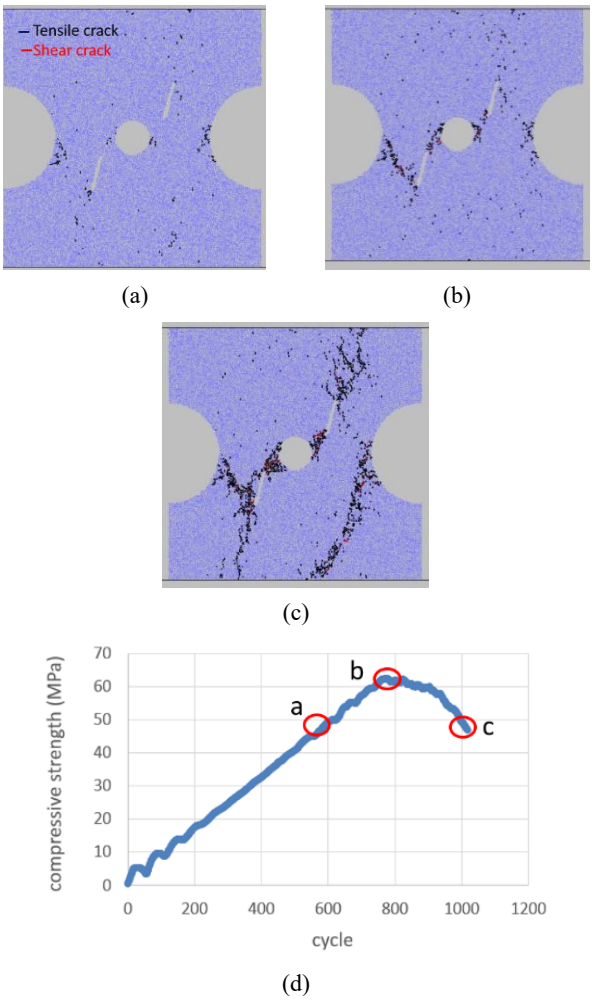

Fig. 22 Crack evolution in specimen containing two echelon joint with angle of 15° during the three stages of the test; (a) crack initiation stress, (b) peak stress, (c) post peak; oriented plane angle was equal to 60°. (d) Variation of compressive strength versus the cycle

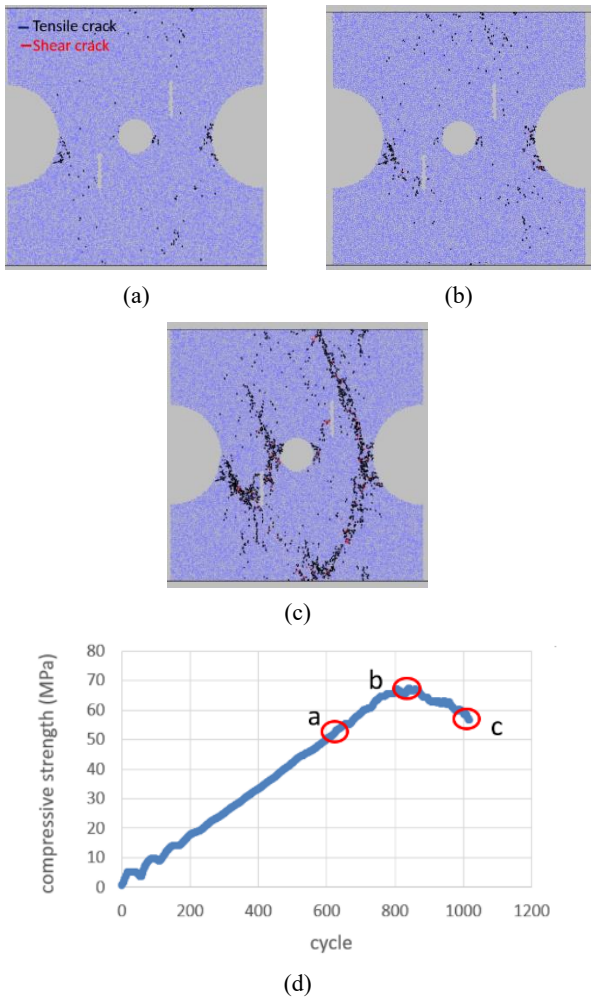

Fig. 23 Crack evolution in specimen containing two echelon joint with angle of 30° during the three stages of the test; (a) crack initiation stress, (b) peak stress, (c) post peak; oriented plane angle was equal to 60°. (d) Variation of compressive strength versus the cycle

c-2) joint angle was 30°

Figs. 23(a)-(c) shows the failure mechanism of specimens with oriented plane angle of 60° and joint angle of 30° in three stages of loading i.e., crack initiation stress stage, final stress stage and post peak stress stage. Red line and black line was representative of shear crack and tensile crack, respectively. Fig. 23(d) shows the variation compressive stress versus the cycle. Three loading stages were highlighted in this figure. In crack initiation stage (Fig. 23(a)), two tensile wing crack initiate from hole walls and propagate diagonally inside the model. In this stage oscillation start in the stress curve ("a" in Fig. 23(d)). In peck stress stage (Figs. 23(b) and (d)), two tensile wing crack initiate from outer tips of joints and propagate diagonally till coalescence with model boundary. Also, two tensile wing crack initiate from inner tips of joints and propagate diagonally till coalescence with hole boundary. In final stage (Figs. 23(c) and (d)), two tensile wing cracks initiate preexisting joints and propagate parallel to loading axis till coalescence with model boundary.\

c-3) joint angle was 45°

Figs. 24(a)-(c) shows the failure mechanism of specimens with oriented plane angle of 60° and joint angle of 45° in three stages of loading i.e., crack initiation stress stage, final stress stage and post peak stress stage. Red line and black line was representative of shear crack and tensile crack, respectively. Fig. 24(d) shows the variation compressive stress versus the cycle. Three loading stages were highlighted in this figure. In crack initiation stage (Fig. 24(a)), two tensile wing crack initiate from hole walls and propagate diagonally inside the model. In this stage oscillation start in the stress curve ("a" in Fig. 24(d)). In peck stress stage (Figs. 24(b) and (d)), two tensile wing crack initiate from outer tips of joints and propagate diagonally till coalescence with model boundary. Also, two tensile wing crack initiate from inner tips of joints and propagate diagonally till coalescence with hole boundary. In final stage (Figs. 24(c) and (d)), two tensile wing cracks initiate preexisting joints and propagate parallel to loading axis till coalescence with model boundary.

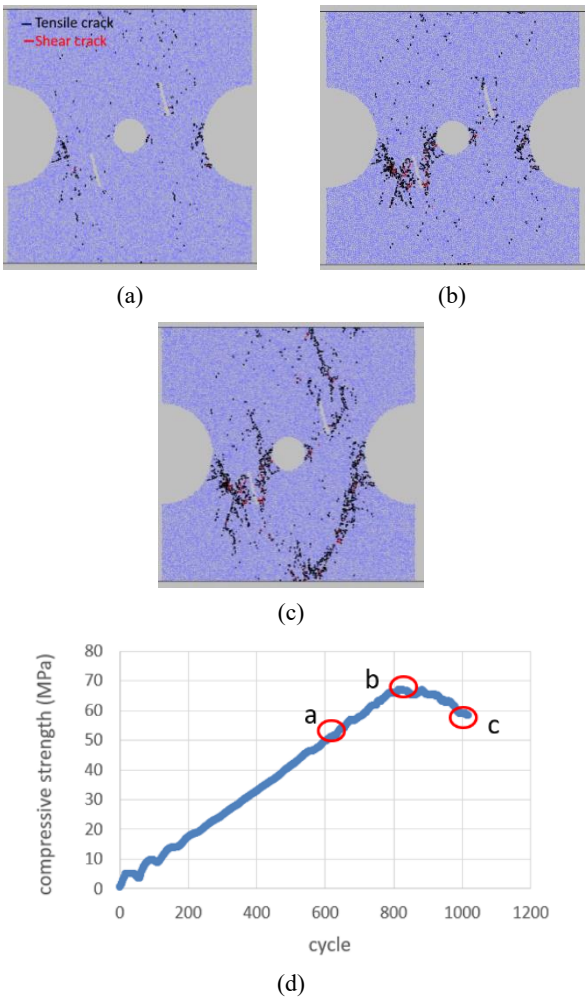

Fig. 24 Crack evolution in specimen containing two echelon joint with angle of 30° during the three stages of the test; (a) crack initiation stress, (b) peak stress, (c) post peak; oriented plane angle was equal to 60°. (d) Variation of compressive strength versus the cycle

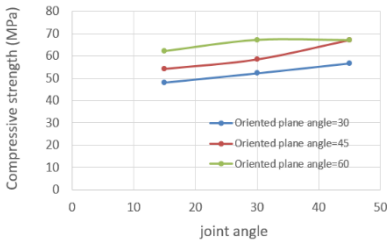

Fig. 25 The effect of joint angle on the strength of models

By comparison between Figs. 5-7 and Figs. 16-24, It can be concluded that failure pattern is similar in both of the experimental test and numerical simulation.

4.6 The effect of oriented plane angle and joint angle on the strength of samples

Fig. 25 shows the effect of oriented plane angle and joint angle on the strength of models. This figure was presented for three oriented plane angles.

The strength of samples was increased by increasing the joint angle. Also, the strength of sample was increased by increasing the oriented plane angle.

By comparison between Figs. 8 and 25, it can be concluded that failure strength is nearly similar in both of the experimental test and numerical simulation.

5. Conclusions

Experimental and discrete element methods were used to investigate the effects of both of the non-persistent joints and hole on the failure behaviour of rock pillars under uniaxial compressive test. concete samples with dimension of 150 mm × 150 mm × 50 mm were prepared. Within the specimen, two echelon non-persistent notches and one hole were provided. The hole was inserted at the middle of the specimen. two joints were distributed on the three diagonal planes. the angle of diagonal plane related to horizontal axis were 15°, 30° and 45°. The angle of joints related to diagonal plane were 30°, 45°, 60°. Totally, 9 different configuration systems were prepared. In these configurations, the length of joints was taken as 20 mm. diameter of hole was 20 mm. Similar to those for joints configuration systems in the experimental tests, 9 models with different echelon non-persistent joint were prepared in numerical model. The axial load was applied to the model by rate of 0.05 mm/min. The results shows that:

- Oriented plane angle was 30°

When joint angle was 15°, two tensile wing cracks initiated from outer joint tips and propagated diagonally related to loading axis till coalescence with boundaries of sample. Also, two wing crack initiate from inner joint tips and propagates diagonally till coalescence with the hole wall. Two vertical tensile cracks initiate from the joint walls and propagate parallel to loading axis till coalescence with sample boundary. When joint angle was 30°, one tensile wing cracks initiated from outer tip of left joint and propagated diagonally related to loading axis till coalescence with boundaries of sample. Also, two vertical tensile cracks initiate from the joint walls and propagate parallel to loading axis till coalescence with sample boundary. When joint angle was 45°, one tensile wing cracks initiated from outer tip of right joint and propagated diagonally related to loading axis till coalescence with boundaries of sample. Also, two vertical tensile cracks initiate from the joint walls and propagate parallel to loading axis till coalescence with sample boundary. In this condition, the rock bridges were broken during the test. Failure surface was smooth without pulverized material. This is representative of tensile crack.

- Oriented plane angle was 45°

When joint angle was 15°, two tensile wing cracks initiated from inner joint tips and propagated diagonally related to loading axis till coalescence with boundaries of hole. Two vertical tensile cracks initiate from the joint walls and propagate parallel to loading axis till coalescence with sample boundary. When large joint angle was 30°, two

tensile wing cracks initiated from outer joint tips and propagated diagonally related to loading axis till coalescence with boundaries of sample. Also, two wing crack initiate from inner joint tips and propagates diagonally till coalescence with the hole wall. When large joint angle was 45°, two tensile wing cracks initiated from inner joint tips and propagated diagonally related to loading axis till coalescence with boundaries of hole. Two vertical tensile cracks initiate from the joint walls and propagate parallel to loading axis till coalescence with sample boundary. In these conditions, the rock bridges were broken during the test. Failure surface was smooth without pulverized material. This is representative of tensile crack.

- Oriented plane angle was 60°

When joint angle was 15°, two tensile wing cracks initiated from outer joint tips and propagated diagonally related to loading axis till coalescence with boundaries of sample. Also, two wing crack initiate from inner joint tips and propagates diagonally till coalescence with the hole wall. Two vertical tensile cracks initiate from the joint walls and propagate parallel to loading axis till coalescence with sample boundary. When joint angle was 30°, one tensile wing cracks initiated from outer tip of left joint and propagated diagonally related to loading axis till coalescence with boundaries of sample. Also, two vertical tensile cracks initiate from the joint walls and propagate parallel to loading axis till coalescence with sample boundary. When joint angle was 45°, one tensile wing cracks initiated from outer tip of right joint and propagated diagonally related to loading axis till coalescence with boundaries of sample. Also, two vertical tensile cracks initiate from the joint walls and propagate parallel to loading axis till coalescence with sample boundary. In this condition, the rock bridges were broken during the test. Failure surface was smooth without pulverized material. This is representative of tensile crack.

- The wing crack angle related to joint plane decrease by increasing the joint angle.
- The strength of samples was increased by increasing the joint angle.
- The strength of sample was increased by increasing the oriented plane angle.
- The failure pattern is similar in both of the experimental test and numerical simulation.
- Failure strength is similar in both of the experimental test and numerical simulation.
- The number of tensile cracks increase by increasing the oriented plane angle.
- The number of tensile crack increase by increasing the joint angle.
- The author suggests the study of similar models in other loading rates.

References

Amadei, B. (1988), "Strength of a regularly jointed rock mass under biaxial and axisymmetric loading conditions", *Int. J. Rock Mech. Min Sci.*, **25**(3), 3-13. https://doi.org/10.1016/0148-9062(88)92712-X

Coli, N., Berry, P. and Boldini, D. (2011), "In situ nonconventional shear tests for the mechanical characterization of a bimrock", *Int. J. Rock Mech. Min. Sci.*, **48**, 95-102. https://doi.org/10.1016/j.ijrmms.2010.09.012

Cook, N.G.W. (1976), "Seismicity associated with mining", *Eng. Geol.*, **10**, 99-122. https://doi.org/10.1016/0013-7952(76)90015-6

Cundall, P.A. and Strack, O.D.L. (1979), "A discrete numerical model for granular assemblies", *Geotechnique*, **29**(1), 47-65. https://doi.org/10.1680/geot.1979.29.1.47

Esmaieli, K., Hadjigeorgiou, J. and Grenon, M. (2010), "Estimating geometrical and mechanical REV based on synthetic rock mass models at Brunswick Mine", *Int. J. Rock Mech. Min. Sci.*, **47**(6), 915-926. https://doi.org/10.1016/j.ijrmms.2010.05.010

Fang, Z. and Harrison, J.P. (2002), "Numerical analysis of progressive fracture and associated behaviour of mine pillars by use of a local degradation model", *Trans. Instn. Min. Metal.*, **111**, 59-72. https://doi.org/10.1179/mnt.2002.111.1.59

Gerrard, C.M. (1982), "Elastic models of rock masses having one, two and three sets of joints", *Int. J. Rock Mech. Min Sci.*, **19**, 15-23. https://doi.org/10.1016/0148-9062(82)90706-9

Ghazvinian, A., Sarfarazi, V., Schubert, W. and Blumel, M. (2012), "A study of the failure mechanism of planar non-persistent open joints using PFC2D", *Rock Mech. Rock Eng.*, **45**(5), 677-693. https://doi.org/10.1007/s00603-012-0233-2

Hoek, E. and Brown, E.T. (1997), "Practical estimates of rock mass strength", *Int. J. Rock Mech. Min. Sci.*, **34**(8), 1165-1186. https://doi.org/10.1016/S1365-1609(97)80069-X

Halakatevakis, N. and Sofianos, A. (2010), "Strength of a blocky rock mass based on an extended plane of weakness theory", *Int. J. Rock Mech. Min Sci.*, **47**(4), 568-582. https://doi.org/10.1016/j.ijrmms.2010.01.008

Haeri, H. and Sarfarazi, V. (2016a), "The effect of micro pore on the characteristics of crack tip plastic zone in concrete", *Comput. Concrete, Int. J.*, **17**(1), 107-112. https://doi.org/10.12989/cac.2016.17.1.107

Haeri, H. and Sarfarazi, V. (2016b), "The effect of non-persistent joints on sliding direction of rock slopes", *Comput. Concrete, Int. J.*, **17**(6), 723-737. https://doi.org/10.12989/cac.2016.17.6.723

Haeri, H. and Sarfarazi, V. (2016c), "The deformable multilaminate for predicting the elasto-plastic behavior of rocks", *Comput. Concrete, Int. J.*, **18**, 201-214. https://doi.org/10.12989/cac.2016.18.2.201

Haeri, H., Sarfarazi, V. and Lazemi, H.A. (2016d), "Experimental study of shear behavior of planar non-persistent joint", *Comput. Concrete, Int. J.*, **17**(5), 639-653. https://doi.org/10.12989/cac.2016.17.5.649

Halakatevakis, N. and Sofianos, A. (2010), "Strength of a blocky rock mass based on an extended plane of weakness theory", *Int. J. Rock Mech. Min Sci.*, **47**(4), 568-582. https://doi.org/10.1016/j.ijrmms.2010.01.008

Ivars, D.M., Pierce, M.E., Darcel, C., Reyes-Montes, J., Potyondy, D.O., Young, R.P. and Cundall, P.A. (2011), "The synthetic rock mass approach for jointed rock mass modelling", *Int. J. Rock Mech Min Sci.*, **48**(2), 219-244. https://doi.org/10.1016/j.ijrmms.2010.11.014

Khani, A. (2013), "Numerical investigation of the effect of fracture intensity on deformability and REV of fractured rock masses", *Int. J. Rock Mech. Min. Sci.*, **63**, 104-112. https://doi.org/10.1016/j.ijrmms.2013.08.006

Khani, A., Baghbanan, A., Norouzi, S. and Hashemolhosseini, H. (2013), "Effects of fracture geometry and stress on the strength of a fractured rock mass", *Int. J. Rock Mech. Min. Sci.*, **60**, 345-352. https://doi.org/10.1016/j.ijrmms.2013.01.011

Kulatilake, H. and Stephansson, O. (1994), "Effect of finite size joints on the deformability of jointed rock at the two

dimensional level", *Can. Geo. Tech. J.*, **31**, 364-374. https://doi.org/10.1139/t94-044

Lin, Q., Cao, P., Cao, R., Lin, H. and Meng, J. (2020), "Mechanical behaviour around double circular openings in a jointed rock mass under uniaxial compression", *Arch. Civil Mech. Eng.*, **20**(1), 19. https://doi.org/10.1007/s43452-020-00027-z

Martina, C.D. and Maybee, W.G. (2000), "The strength of hard-rock pillars", *Int. J. Rock Mech. Min. Sci.*, **37**, 1239-1246. https://doi.org/10.1016/S1365-1609(00)00032-0

Min, K.B. and Jing, L. (2003), "Numerical determination of the equivalent elastic compliance tensor for fractured rock masses using the distinct element method", *Int. J Rock Mech. Min Sci.*, **40**(6), 795-816. https://doi.org/10.1016/S1365-1609(03)00038-8

Özkan, İ., Erdem, B.Ü.L.E.N.T. and Ceylanoğlu, A. (2015), "Characterization of jointed rock masses for geotechnical classifications utilized in mine shaft stability analyses", *Int. J. Rock Mech. Min. Sci.*, **73**, 28-41. https://doi.org/10.1016/j.ijrmms.2014.10.001

Palmstrom, A. and Singh, R. (2001), "The deformation modulus of rock masses: comparisons between in situ tests and indirect estimates", *Tunnel. Undergr. Space Technol.*, **16**, 115-131. https://doi.org/10.1016/S0886-7798(01)00038-4

Potyondy, D.O. and Cundall, P.A. (2004), "A bonded-particle model for rock", *Int. J. Rock Mech. Min. Sci.*, **41**, 1329-1364. https://doi.org/10.1016/j.ijrmms.2004.09.011

Protosenya, A. and Verbilo, P. (2016), "Forecast Jointed Rock Mass Compressive Strength Using a Numerical Model", *MATEC Web of Conferences*, Volume 73, Article number 04006.

Ranjith, P.G., Fourar, M., Pong, S.F., Chian, W. and Haque, A. (2004), "Characterization of fractured rocks under uniaxial loading states", *Int. J. Rock Mech. Min. Sci.*, **41**, 43-48. https://doi.org/10.1016/j.ijrmms.2004.03.017

Sarfarazi, V. and Haeri, H. (2016), "Effect of number and configuration of bridges on shear properties of sliding surface", *J. Min. Sci.*, **52**(2), 245-257. https://doi.org/10.1134/S1062739116020370

Sarfarazi, V., Ghazvinian, A., Schubert, W., Blumel, M. and Nejati, H.R. (2014), "Numerical simulation of the process of fracture of Echelon rock joints", *Rock Mech. Rock Eng.*, **47**(4), 1355-1371. https://doi.org/10.1007/s00603-013-0450-3

Sarfarazi, V., Faridi, H.R., Haeri, H. and Schubert, W. (2016), "A new approach for measurement of anisotropic tensile strength of concrete", *Adv. Concrete Constr., Int. J.*, **3**(4), 269-284. https://doi.org/10.12989/acc.2015.3.4.269

Sarfarazi, V., Haeri, H., Shemirani, A. and Zhu, Z. (2017), "Shear behavior of non-persistent joint under high normal load". *Strength Mater.*, **49**, 320-334. https://doi.org/10.1007/s11223-017-9872-6

Wang, P. (2016), "Numerical analysis on scale effect of elasticity, strength and failure patterns of jointed rock masses", *Geosci. J.*, **20**(4), 539-549. https://doi.org/10.1007/s12303-015-0070-x

Yang, J.P., Chen, W.Z., Yang, D.S. and Yuan, J.Q. (2015), "Numerical determination of strength and deformability of fractured rock mass by FEM modeling", *Comput. Geotech.*, **64**, 20-31. https://doi.org/10.1016/j.compgeo.2014.10.011

Yaylaci, M. (2016), "The investigation crack problem through numerical analysis", *Struct. Eng. Mech., Int. J.*, **57**(6), 1143-1156. https://doi.org/10.12989/sem.2016.57.6.1143

Yaylaci, M. and Birinci, A. (2013), "The receding contact problem of two elastic layers supported by two elastic quarter planes", *Struct. Eng. Mech., Int. J.*, **48**(2), 241-255. https://doi.org/10.12989/sem.2013.48.2.241

Yaylacı, M. and Birinci, A. (2015), "Analytical solution of a contact problem and comparison with the results from FEM", *Struct. Eng. Mech., Int. J.*, **54**(4), 607-622. https://doi.org/10.12989/sem.2015.54.4.607

Yaylaci, M. and Avcar, M. (2020), "Finite element modeling of contact between an elastic layer and two elastic quarter planes", *Comput. Concrete, Int. J.*, **26**(2), 107-114. https://doi.org/10.12989/cac.2020.26.2.000

Yaylaci, M., Terzi, C. and Avcar, M. (2019), "Numerical analysis of the receding contact problem of two bonded layers resting on an elastic half plane", *Struct. Eng. Mech., Int. J.*, **72**(6), 775-783. https://doi.org/10.12989/sem.2019.72.6.000

Yaylaci, E.U., Yaylaci, M., Olmez, H. and Birinci, A. (2020), "Artificial neural network calculations for a receding contact problem", *Comput. Concrete, Int. J.*, **25**(6), 551-563. https://doi.org/10.12989/cac.2020.25.6.000

BS